Transformation and Structure of Cation Radicals in L-α-Alanine

T. L. Petrenko*

Institute of Physics of Semiconductors, National Academy of Sciences, Prosp. Nauky 45, Kyiv 03028, Ukraine

Received: February 17, 2001; In Final Form: May 18, 2001

A quantum chemical simulation for radicals of a cation branch in irradiated L-α-alanine crystals was carried out. The large cluster approach was used for investigation of possible paths of radical transformation. Both intermolecular and intramolecular proton transfer together with decarboxylation process were considered. Relative total energies of various radical structures were obtained at the PM3 level followed by DFT calculation of hyperfine parameters for the protons of the corresponding radical. It was shown that in this crystal the radicals R2 and R3 observed by ESR and ENDOR techniques are the products of the transformation of the primary cation radical.

1. Introduction

The formation of radicals in single crystals of L-α-alanine exposed to γ or X-rays, neutrons, electrons, or α particles is the subject of investigation during the past four decades.[1] The growing interest in this crystal is determined, among other things, by the application of alanine for high dose dosimetry devises.[2]

The main experimental techniques for the investigation of radicals structures and their transformations in alanine and related materials are ESR and ENDOR. However, the interpretation of such experiments is rather difficult because of the complexity of the crystal structure and associated spectra. The conventional procedure for the investigation of the radical structure is the determination of tensors of anisotropic hyperfine interaction (AHFI) for various protons of the radiation damage. The spin density therewith is assumed to be located mainly on one of the atoms of the radical. Thus, one may estimate the distance between this atom and proton using the point−dipole approximation. Together with the determination of direction cosines, this procedure gives the position of a particular proton in the crystal lattice. However, in the case of sufficiently delocalized spin density or large lattice relaxation, this approach may give wrong results.

One would expect that the best way for the interpretation of experimental data is the quantum-chemical simulation of radicals using the appropriate method of calculation. The main difficulties are associated with the large size of the active space of the crystal responsible for the radical formation. It is evident that the minimum size of the system required for a proton-transfer investigation is a 91-atom cluster that includes the central molecule and six hydrogen-bonded neighbor molecules

$$C_\beta(H_\beta)_3N(H_N)_3C_\alpha H_\alpha C_C O_2 + 6(CH_3NH_3CHCO_2) \quad (1)$$

where the commonly used subscripts correspond to methyl, nitrogen, alpha, and carboxylic groups. On the other hand, it is well-known that for the correct description of hydrogen bonds the high-level theoretical methods are necessary.[3] So, in practice, the choosing of appropriate approximations is of crucial importance.

Until now, almost all experimental investigations were devoted to the structure and transformations of the anion bunch of radicals. The series of radicals starting with the primary unstable one to the final high-temperature forms were extensively studied.[4−6] Recently, it was determined that three new ENDOR spectra are hidden under the spectrum of a well-known stable radical,[7] and three new stable radical structures were proposed. This experimental investigation was followed by two theoretical papers dealing with density-functional theory (DFT) based calculations of hyperfine interactions (HFI) for isolated forms of these radicals.[8,9] Despite the excellent agreement of calculated hyperfine parameters (HFPs) with experimental ones, it should be mentioned that this agreement is partially the result of the fitting of the dihedral angles values. Besides, the nature of the new stable radicals, their precursors, mechanism of formation is still unknown.

From the fundamental principle of charge conservation, one may expect the generation of both cation branch radicals and anion branch radicals in nearly equal concentrations under irradiation. However, we know only one early work dedicated to the experimental investigation of the low-temperature cation radical in L-α-alanine.[10] One may notice that ESR or ENDOR methods themselves cannot determine the charge of radiation damage. So, the conclusion of ref 10 about the breaking of the $C_\alpha-C_\beta$ bond in cation on the basis of the analysis of strongly overlapped ESR spectra is not trustworthy, and further investigations are required.

In ref 11, the restricted SCF MO INDO calculation for the deprotonated cation radical was carried out. However, the cluster used is too small, and the geometry optimization was not performed. Strictly speaking, such a calculation is inappropriate for comparison with the magnetic resonance experiment.

The present work is devoted to the computer simulation of the cation branch for radicals in irradiated L-α-alanine. We shall start from the primary cation radical in the crystal and then consider various paths of its transformation together with the corresponding energy gain. HFPs are calculated for various radical conformations and compared with the available ESR and ENDOR data.

* To whom correspondence should be addressed. Fax: (38) (044) 265-83-42. E-mail: taraspetrenko@netscape.net.

10.1021/jp0106395 CCC: $22.00
Published on Web 12/12/2001

TABLE 1: Calculated Hydrogen Bond Lengths in the Perfect Crystal, Simulated by a Cluster of 91 Atoms (in Angstroms)[a]

hydrogen bond	MNDO	AM1	PM3	expt[14]
$O^{(1)}-H^{(1)}$	2.84	2.61	1.92	1.86
	2.76	2.09	1.84	
$O^{(2)}-H^{(2)}$	2.37	2.16	1.79	1.78
	2.44	1.92	1.75	
$O^{(2)}-H^{(3)}$	3.96	2.07	1.78	1.83
	2.51	1.88	1.76	

[a] Notations of hydrogen bonds correspond to ref 14.

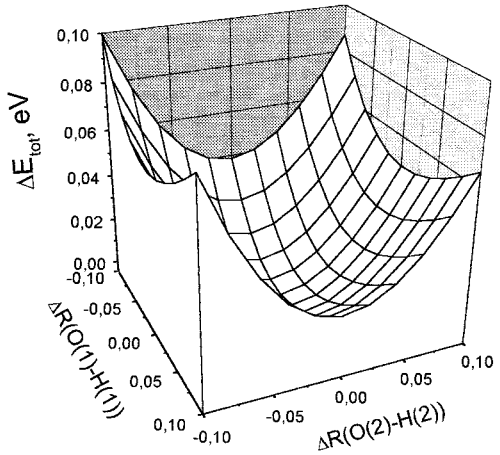

Figure 1. Section of the PES which corresponds to the variation of two hydrogen bond lengths. $\Delta R(O(i)-H(i))$, $i = 1$ or 2, is the deviation of the corresponding distances from the equilibrium values. Notations are similar to the ones in Table 1.

2. Calculation Procedure

The general strategy of calculation includes two steps. The first one is the determination of the equilibrium geometry and total energy for a particular radical conformation using a large cluster, which simulates the active space of the crystal in the framework of an appropriate semiempirical method. The second step is the calculation of HFPs for the obtained geometry using a suitable high level method, which is applied only for the radical, and ignoring the surrounding molecules. The first step includes several important points: choosing the semiempirical method, choosing the boundary conditions for surface atoms, and excluding the wrong solutions for the electronic wave function because of surface effects.

To check the validity of the MNDO, AM1, and PM3 semiempirical methods, we perform the test calculation for the cluster of seven molecules (1). For this purpose, we fix the positions of six surrounding molecules in the host lattice sites and perform the geometry optimization for central molecule only. Table 1 shows the calculated hydrogen bond lengths as compared to experimental ones (notice that symmetry equivalent hydrogen bonds in a perfect crystal become inequivalent in the cluster). It is evident that PM3 parametrization is best suited to reproducing the geometry of the perfect crystal. It should be stressed that we deal with very flat a potential energy surface (PES), associated with hydrogen bond lengths. The reason is that the hydrogen bond occurs between *neutral* molecules. Figure 1 is the qualitative illustration of the behavior of the PES near the equilibrium values of hydrogen bonds. This section of PES was calculated at the PM3 level for a 91-atom cluster (1), with six surrounding molecules being fixed at host lattice positions and the relaxed atoms of the central molecule. For the *charged* species under consideration, such as cations or anions, one may expect a steeper PES and, thus, a more precise calculation of the geometry in the vicinity of radiation damage.

To calculate more reliable values, we hereafter use the cluster of one central and 12 surrounding molecules (a total of 208 atoms) for all subsequent semiempirical calculations. In all cases, we perform partial geometry optimization in internal coordinates with some surface atoms of cluster fixed. The criterion for the selection of such atoms is as follows: if a given atom forms a hydrogen bond in the perfect crystal but this bond is broken in the cluster by artificial means, then a given atom is fixed during total energy minimization. Thus, we fix 13 oxygen atoms and 24 hydrogen atoms on the surface of the cluster. Besides, the rotation of the methyl groups is allowed only for the central molecule. For this purpose, we fix the dihedral angles $H_\beta-C_\beta-C_\alpha-N$ for 12 surrounding molecules at the perfect crystal values.

Our experience with calculations for such clusters reveals some problems. They appear because there are a number of solutions for the electronic wave function which correspond to the localization of spin density on different molecules of the cluster with a net charge +1. If one starts with the standard diagonal density matrix as the guess, the solution with spin density localized on the molecule, located on the surface of cluster, is usually obtained. However, for the simulation of radicals in an alanine crystal, only the solution with the spin density localized on the central molecule of cluster is reasonable. One way to solve this problem is to write an appropriate guess matrix "by hand". In the present calculation, we have to use another more simple empirical procedure. We set the initial value of the $C_\alpha-C_C$ bond length for the central molecule equal to 2.5 Å. This leads to the proper spin density localization on this molecule. Then we reduce this bond length as the reaction coordinate with the step of 0.1 Å until its normal value is reached. At each step, we use the density matrix from the previous calculation as the guess. In such a manner, we obtain the so-called primary cation radical. For all subsequent semiempirical calculations, we use the density matrix from one of the appropriate preceding calculations as the guess to exclude undesired solutions.

The final DFT ab initio calculation of HFPs is performed using the Gaussian 94 code.[12] The 6-311G(d) basis with six d functions and Becke's three-parameter functional including both local and nonlocal terms (B3LYP)[13] is applied. The isotropic constant of HFI a_{iso} and components T_{ij} of the spurless tensor of AHFI with nucleus N are calculated according to the relations

$$a_{iso}^{(N)} = \frac{4\pi}{3} g\beta g_N \beta_N \langle S_z \rangle^{-1} \sum_{\mu\nu} \rho_{\mu\nu} \phi_\mu(r_N) \phi_\nu(r_N) \qquad (2)$$

$$T_{ij}^{(N)} = \frac{1}{2} g\beta g_N \beta_N \langle S_z \rangle^{-1} \sum_{\mu\nu} \rho_{\mu\nu} \langle \phi_\mu(r_k) | r_{kN}^{-5} (r_{kN}^2 \delta_{ij} - 3 r_{kN,i} r_{kN,j}) | \phi_\nu(r_k) \rangle \qquad (3)$$

where ϕ_μ and ϕ_ν run over all basis functions of the particular radical and $\rho_{\mu\nu}$ is the spin density matrix.

3. Results of the Calculations

After the irradiation of a perfect crystal, the hole is captured by an alanine molecule, and a primary cation radical with an associated net charge of +1 is formed. It seems reasonable that

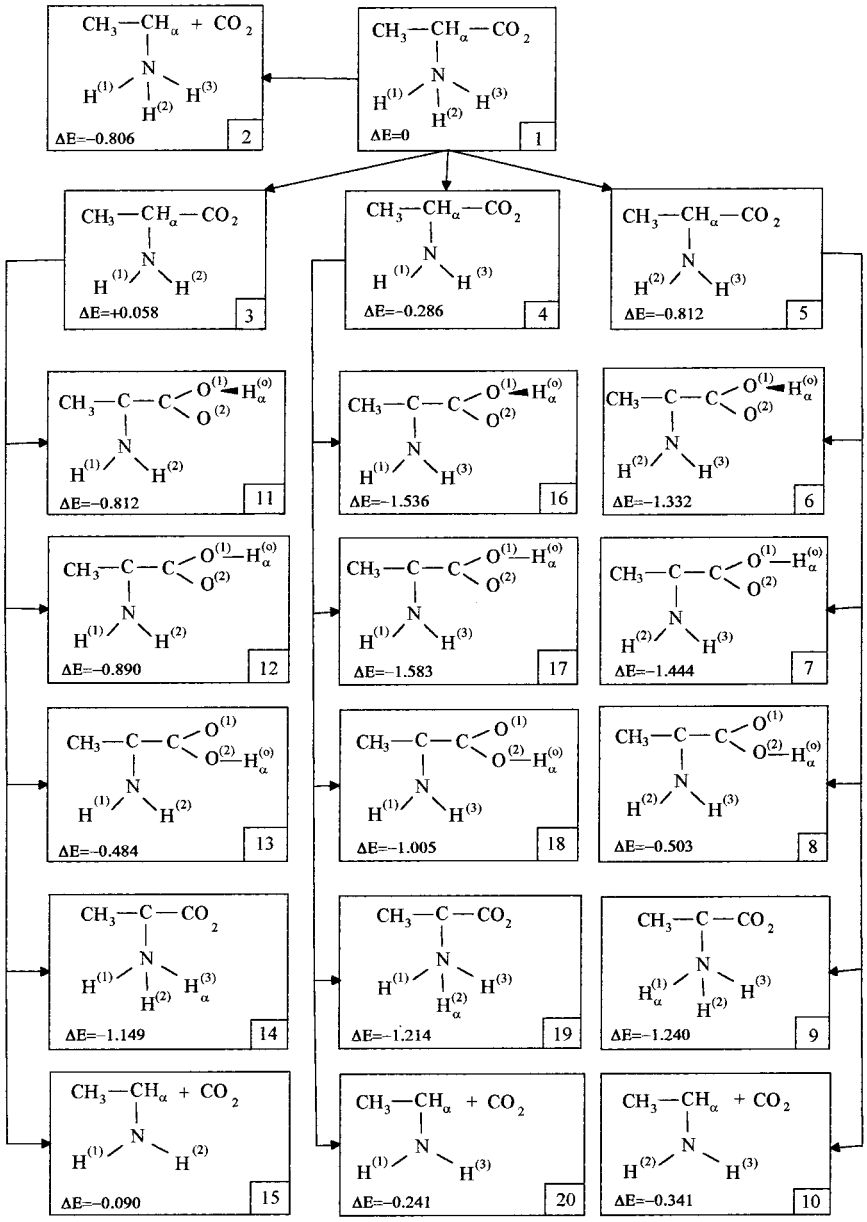

Figure 2. Schematic representation of the radical transformations for the cation branch in L-α-alanine. Δ*E* is the difference in total energies of the particular radical and the primary radical **1** in the 208-atom cluster (in eV), calculated at the PM3 level.

such a radical is unstable and may be long living only at low temperatures similar to the primary anion radical.[4] "Chemical intuition" and experimental ENDOR data[7] suggest that intermolecular and intramolecular proton transfer together with the decarboxylation process may be responsible for the subsequent transformations of the primary cation radical **1** in Figure 2. As a first step, one may suppose the decarboxylation of this radical and the creating of radical **2** or the transfer of one of the amino protons to the neighbor molecule along the corresponding hydrogen bond direction (structures **3**−**5** in Figure 2). As this takes place, the transferred amino proton becomes bonded to the oxygen of the neighbor molecule with $H^{(i)}$ attached to $O^{(i)}$, $i = 1-3$, if one uses the designations of ref 14. Calculations at the PM3 level show that, for radicals **3**−**5**, the positive unity charge is localized on the neighbor molecule, which trapped the transferred proton. At the same time, the spin density is localized practically on these radicals. The same is true also for the radicals formed from deprotonated primary radicals **3**−**5** in subsequent transformations. The above calculations justify the final single-point ab initio DFT calculation of HFPs for neutral radicals, ignoring surrounding molecules. However, one may expect the strong influence of the crystal field on the calculated HFPs of radical through the dihedral angles,[8,9] which are the "soft" coordinates. So, the quality of the calculated HFPs may be regarded as the test for the validity of geometry optimization at the PM3 level.

For the correct comparison of calculated HFPs for β protons with ENDOR experimental data,[7] we consider the limit of rapid rotation in the framework of the expanded Bloch equations.[15] We notice that the usual way to obtain the components of a tensor of HFI for a particular nucleus k is the analysis of angular dependencies of ENDOR frequencies $\nu^{(k)}$ in three mutually perpendicular planes (if there are no symmetry simplifications):

$$\nu_{\pm}^{(k)} = \sqrt{\sum_{m,n} C_{mn}^{(k)} l_m l_n} \tag{4}$$

$$C_{mn}^{(k)} = \sum_{j} B_{mj}^{(k)} B_{nj}^{(k)} \tag{5}$$

$$B_{mj}^{(k)} = \pm \frac{A_{mj}^{(k)}}{2} + \nu_N \delta_{mj} \quad (6)$$

where m, n, and j equal x, y, or z; $l_i = \cos \theta_i$ are the direction cosines of the magnetic field with respect to crystal coordinate system x, y, and z; $h\nu_N = g_N\beta_N H$ is the Larmor frequency for the proton; and $A_{mj}^{(k)}$ is the tensor of HFI. Two ENDOR frequencies ν_+ and ν_- correspond to $M_S = -1/2$ and $+1/2$, respectively.

Thus, under the rapid rotation condition the observed ENDOR frequency is

$$\nu_\pm^{(av)} = \frac{1}{3}[\nu_\pm^{(\beta_1)} + \nu_\pm^{(\beta_2)} + \nu_\pm^{(\beta_3)}] \quad (7)$$

where $\nu^{(\beta_i)}$, $i = 1-3$, corresponds to the ENDOR frequency for the ith methyl proton at equilibrium geometry in the absence of rotation.

It follows from eqs 4−6 that in this case *there is no* simple averaging for the components of the tensor $A_{mj}^{(k)}$ similar to frequencies. Thus, we use the following procedure to find the effective rotationally averaged tensor of HFI for methyl protons, which is suitable for the comparison with the experiment: (i) an ab initio calculation of the HFI tensor $A_{mj}^{(k)}$, $k = 1-3$, for all methyl protons and geometry obtained at the PM3 level, (ii) the calculation according to (4) and (7) of the average value of ENDOR frequency $\nu^{(av)}(l_x, l_y, l_z)$ for the given direction of the magnetic field with respect to the crystal axes, (iii) the calculation of "theoretical angular dependencies" for the values $\nu^{(av)}(l_x, l_y, l_z)$ in planes xy, xz, and yz, and (iv) the fitting of the elements of the effective rotationally averaged tensor $A_{mj}^{(av)}$ in eqs 4−6 to satisfy the calculated "theoretical angular dependencies".

Such procedure is quite similar to the one commonly used for calculation of tensors of HFI from experimental data. The only exception is that we use the calculated angular dependencies of ENDOR frequencies instead of the measured ones.

Generally speaking, we must consider both branches of ENDOR frequencies ν_+ and ν_-. However, our calculations show that sometimes, for the branch with lower ENDOR frequencies, one may find a poor description of the theoretical angular dependencies by relation (4) with tensor $A_{mj}^{(av)}$, as it is shown in Figure 3 in the case of radical **17** (vide infra). At the same time, for the higher ENDOR frequency branch, the description of theoretical angular dependencies in terms of $A_{mj}^{(av)}$ is always very good. So, the calculated data in Table 2 correspond to the above procedure. One may point out that the experimental data in ref 7 also refer to higher ENDOR frequencies.

From the data in Table 2, we can draw the conclusion that in most cases the fitted HFPs are equal to the ones obtained by simple averaging:

$$A_{mm}^{(av)} = \frac{1}{3}(A_{mm}^{(1)} + A_{mm}^{(2)} + A_{mm}^{(3)}) \quad (8)$$

However, in the case of relatively small values of elements of the tensor of HFI, one may observe the noticeable distinction between the results of such procedures.

4. Discussion

In this section, we will give the brief description of radicals represented schematically in Figure 2 and consider possible assignment of radicals R2 and R3 investigated by ENDOR.[7]

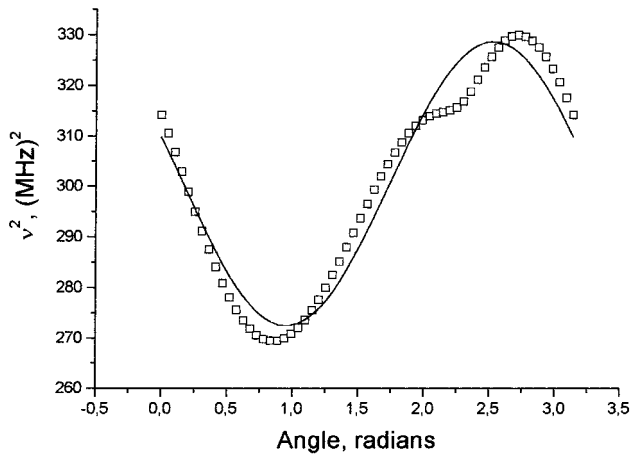

Figure 3. Example of poor description of angular dependence of averaged ENDOR frequency ($M_S = -1/2$) for beta protons of radical **17**. Open squares correspond to calculations according to (4) and (7), and the solid line is the fitted curve.

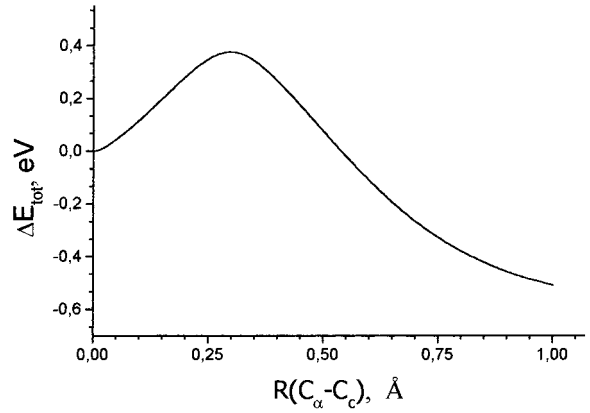

Figure 4. Potential barrier for the decarboxylation process for radical **1** vs the distance between atoms C_α and C_c.

Radical 1. It is the primary cation radical formed immediately after the capture of the hole during irradiation. The unity positive charge is totally localized on this radical, and spin density is localized mainly on two oxygens. The structure of this radical is close to the structure of the undamaged alanine molecule in the host crystal.

Radical 2. The second possible radical form may be generated from radical **1** after shifting the C_cO_2 group and overcoming of the potential barrier of 0.4 eV calculated at the PM3 level. The $C_\alpha-C_c$ bond becomes broken, and its length is nearly 3.5 Å. The unity positive charge and spin density are spread over the fragment $CH_3-CH_\alpha-NH_3$, whereas the fragment CO_2 is uncharged and nonparamagnetic. This radical is most likely unobservable because of the relatively high total energy. The other reason is a relatively low potential barrier transparency as compared to the one for proton transfer because of the great difference in masses. Figure 4 represents the potential barrier, which is necessary to overcome, calculated at the PM3 level. One may also notice that radical **2** cannot be assigned to radical R2[7] (see Table 2) because of the predicted relatively large HFI with H_α protons. Thus, the most probable next step is the amino proton transfer from primary radical **1** to the neighbor alanine molecule along the corresponding hydrogen bond.

Radicals 3−5. These radicals are the deprotonated forms of the primary radical **1**. The distinctions of one radical from another are caused by selective proton transfer along one of

TABLE 2: Calculated HFPs (in MHz) for Magnetic Nuclei of Various Alanine Radicals[a]

number of radical	HFP	H_α	beta protons				N	Amino protons			$H^{(o)}$
			$H_\beta^{(1)}$	$H_\beta^{(2)}$	$H_\beta^{(3)}$	$H_\beta^{(av)}$		$H^{(1)}$	$H^{(2)}$	$H^{(3)}$	
1	a_{iso}	5.2	0.14	0.38	−1.2	−0.22 (−0.23)	2.5	−0.05	1.8	−0.29	
	T_{11}	6.1	5.2	3.3	1.3	2.9 (3.3)	0.59	6.0	2.8	3.1	
	T_{22}	−1.3	−1.6	−0.57	0.08	−0.85 (−0.70)	−0.15	−2.7	−0.83	−0.86	
2	a_{iso}	−72.5	38.4	45.1	175.9	86.6 (86.5)	−8.4	38.3	98.9	18.9	
	T_{11}	38.7	9.8	10.8	14.3	8.0 (11.6)	0.78	12.3	15.8	12.7	
	T_{22}	−2.2	−2.3	−2.8	−5.8	−2.1 (−3.6)	−0.23	−3.8	−7.4	−3.4	
3	a_{iso}	30.0	5.1	3.2	−0.45	2.6 (2.6)	6.9	−13.0	−13.1		
	T_{11}	6.0	4.3	2.7	3.9	3.2 (3.6)	18.1	13.6	11.5		
	T_{22}	−1.1	−1.2	−0.83	−1.4	−1.2 (1.1)	−8.9	−2.7	−0.85		
4	a_{iso}	30.0	5.1	−1.5	1.3	1.6 (1.6)	12.4	−20.9		−21.5	
	T_{11}	6.2	5.5	1.4	2.6	2.8 (3.2)	29.0	22.8		21.2	
	T_{22}	0.33	−1.6	0.39	−0.15	−0.42 (−0.45)	−14.3	−5.1		−4.2	
5	a_{iso}	11.7	−0.68	−1.0	0.90	−0.27 (−0.26)	9.1		−13.5	−13.5	
	T_{11}	6.2	3.4	1.1	2.9	2.2 (2.5)	20.6		17.3	14.3	
	T_{22}	0.83	−1.0	0.12	−0.62	−0.72 (−0.5)	−10.0		−3.9	−2.1	
6	a_{iso}		72.0	1.2	73.5	48.9 (48.9)	15.3		−6.5	18.8	1.3
	T_{11}		6.9	6.9	11.3	6.5 (8.4)	23.1		25.9	24.4	5.6
	T_{22}		−1.7	−2.0	−5.2	−2.2 (−3.0)	−11.1		−9.7	−8.0	−2.0
7	a_{iso}		69.0	2.7	95.9	55.9 (55.9)	13.2		−12.1	21.8	−1.8
	T_{11}		12.9	9.0	9.9	8.8 (10.6)	24.4		27.4	24.3	7.9
	T_{22}		−5.5	−2.3	−3.1	−3.5 (−3.6)	−12.0		−10.5	−7.1	−2.1
8	a_{iso}		30.6	86.5	12.6	43.3 (43.2)	16.6		−3.8	7.1	−2.3
	T_{11}		9.9	8.1	7.9	6.8 (8.6)	23.9		26.3	25.2	4.6
	T_{22}		−4.2	−3.2	−2.5	−2.9 (−3.3)	−11.7		−8.7	−8.9	−1.4
9	a_{iso}		31.9	124.6	34.9	63.8 (63.8)	−4.5	34.3	17.4	72.6	
	T_{11}		8.5	13.3	7.5	7.8 (9.8)	0.76	9.0	9.5	14.3	
	T_{22}		−2.0	−6.3	−1.3	−2.6 (−3.2)	−0.20	−1.8	−1.8	−6.4	
11	a_{iso}		7.5	63.3	32.4	34.4 (34.4)	6.6	−16.6	−19.1		−1.3
	T_{11}		6.2	8.9	7.9	6.8 (7.7)	23.7	20.0	20.7		4.6
	T_{22}		−2.0	−2.9	−2.4	−3.3 (−2.4)	−11.5	−5.9	−6.4		−1.2
12	a_{iso}		8.9	80.2	35.4	41.5 (41.5)	5.3	−12.6	−18.4		1.2
	T_{11}		7.6	7.3	8.9	6.6 (7.9)	24.0	18.9	21.1		4.9
	T_{22}		−2.0	−2.7	−2.8	−2.6 (−2.5)	−11.8	−4.6	−6.0		−1.9
13	a_{iso}		57.0	53.2	0.38	36.9 (36.9)	6.1	−18.3	−20.6		−2.9
	T_{11}		7.8	9.4	7.2	6.5 (8.1)	26.2	19.8	21.7		4.2
	T_{22}		−2.8	−3.8	−2.6	−2.6 (−3.1)	−12.8	−6.0	−6.1		−0.93
14	a_{iso}		93.0	132.1	5.5	76.9 (76.9)	−8.0	7.6	91.5	48.7	
	T_{11}		11.3	12.4	8.7	8.1 (10.8)	0.39	10.8	13.9	12.2	
	T_{22}		−3.3	−4.4	−2.9	−2.7 (−3.5)	0.03	−1.8	−4.7	−3.3	
16	a_{iso}		3.7	70.3	44.9	39.7 (39.6)	16.1	−3.4		−4.1	−0.83
	T_{11}		6.4	10.1	8.2	7.3 (8.2)	21.6	23.6		25.4	5.0
	T_{22}		−2.0	−3.2	−2.7	−3.6 (−2.6)	−10.6	−8.8		−10.8	−1.6
17	a_{iso}		4.9	73.6	40.0	39.5 (39.5)	19.2	0.34		−4.5	0.74
	T_{11}		6.3	9.7	8.2	7.2 (8.1)	21.2	24.2		26.9	4.9
	T_{22}		−1.5	−3.0	−2.7	−3.3 (−2.4)	−10.3	−9.4		−12.2	−1.7
18	a_{iso}		61.4	57.4	0.44	39.8 (39.7)	14.5	−14.6		−6.6	−2.9
	T_{11}		8.8	9.0	7.5	6.8 (8.4)	24.9	25.9		23.6	4.1
	T_{22}		−3.3	−3.5	−2.7	−2.8 (−3.2)	−12.2	−9.9		−9.1	−0.91
19	a_{iso}		70.1	121.4	7.4	66.4 (66.3)	−5.6	70.0	66.3	3.2	
	T_{11}		11.1	10.6	8.2	7.8 (10.0)	0.60	12.6	13.4	7.4	
	T_{22}		−3.7	−4.1	−2.5	−3.1 (−3.4)	0.08	−3.1	−4.7	0.36	
R2 (exp.)	a_{iso}					70.8		86.3	30.2	10.2	
	T_{11}					5.3		9.5	10.7	9.7	
	T_{22}					−2.5		−2.7	−4.7	−4.8	
R3 (exp.)	a_{iso}					39.5					
	T_{11}					5.0					
	T_{22}					−2.2					
(R3)′ (exp.)	a_{iso}					33.1					
	T_{11}					4.6					
	T_{22}					−2.3					

[a] T_{11} and T_{22} denote the principal values of the spurless tensor of AHFI. Values in parenthesis are calculated according to eq 8.

the inequivalent hydrogen bonds. These radicals are neutral, and the unity positive charge is transferred to the corresponding neighbor alanine molecule. One may see the significant difference in total energy between these radicals. It is clear that such radicals are similar to the well-known primary anion radical in L-α-alanine.[4]

Radicals 6, 7, 11, 12, 16, and 17. These radicals are the products of the subsequent transformation of radicals **3**−**5**, which appear as the result of α-proton transfer to the $O^{(1)}$ atom in the carboxylic group. There are three pairs of radical conformations that have almost equal total energies. Such conformations differ from each other by the rotation of the $C_cO^{(1)}O^{(2)}$ plane around the $C_\alpha-C_c$ bond and the position of the $H^{(o)}$ proton with respect to the $C_cO^{(1)}O^{(2)}$ plane as it is shown in Figure 5. From the energy considerations, radicals **16** and **17** are the most preferable. For both of these radicals, the

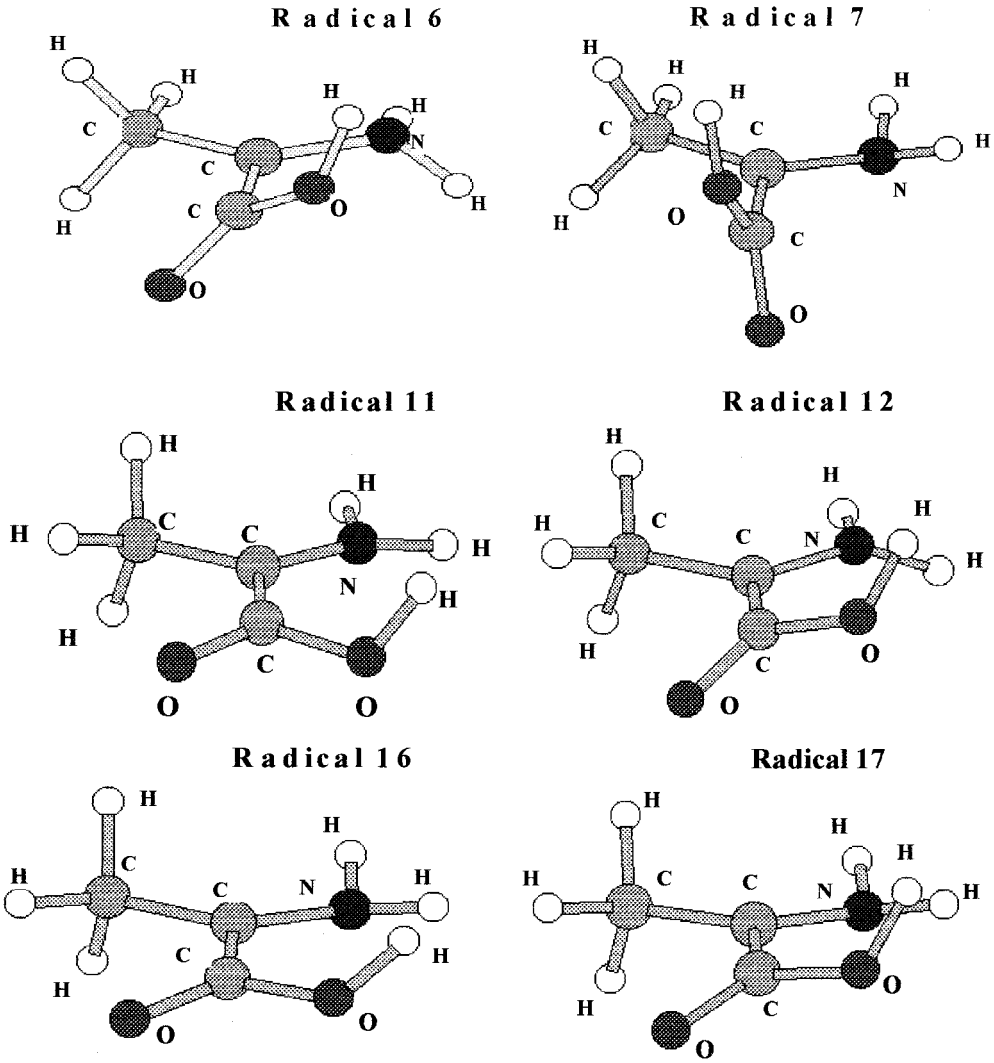

Figure 5. Various conformations of radicals with the H_α proton transferred to $O^{(1)}$.

calculated HFPs for beta protons are rather close to the observed ones for radical R3 as one can see from Table 2. However, it is difficult to assign the observed radical (R3)′; from the energy considerations, radical **7** is more adequate, whereas calculated HFPs suit better to radical **11**. On the one hand, there are not enough experimental data in ref 7 concerning the radicals R3 and (R3)′, and only average data for the methyl protons are available for comparison with calculated data. On the other hand, relatively small errors in the calculated radical geometries may lead to substantial deviation of HFPs and relatively small changes in total energy. So, if the total energy evaluation is the most adequate, it seems reasonable that radicals R3 and (R3)′ may be assigned to radicals **16** and **17**.

Radicals 8, 13, and 18. These radicals are also the products of the transformation of radicals **3**−**5**, except that the α proton is transferred to $O^{(2)}$ instead of $O^{(1)}$. For all of these radicals, the calculated HFPs for methyl protons are rather close to the observed ones for radical R3. However, their total energies are too high, and we believe that these radicals cannot manifest themselves in the experiment.

Radicals 9, 14, and 19. These radicals are generated from radicals **3**−**5** by transferring an α proton to the amino group. The structure of such species is similar to the structure of the observed radical R2.[7] It will be recalled that the unity positive charge is located on the neighbor molecule. The radicals themselves are neutral and contain almost the whole spin

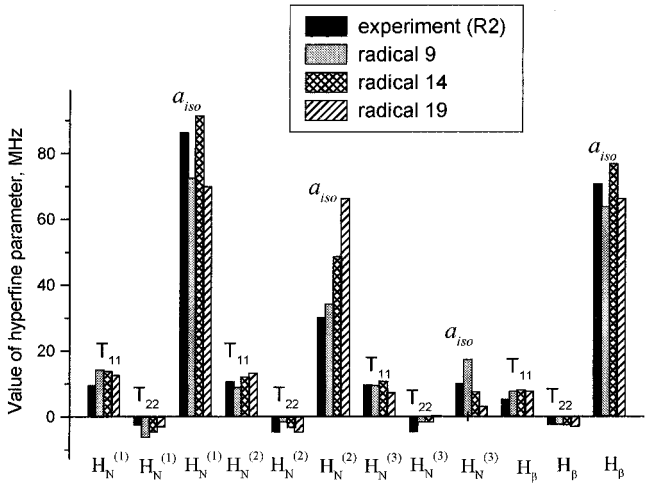

Figure 6. Diagrammatic representation of HFPs for observed radical R2 and calculated ones for possible radical structures.

density. The corresponding total energies are rather close to each other. Thus, to assign radical R2,[7] one must consider, along with energy reasons, the agreement between the calculated and observed HFPs as is shown in Figure 6. For this purpose, we will discuss the degree of quantitative correlation of calculated and observed HFPs for the amino protons $H_N^{(i)}$ ($i = 1-3$) of radical R2.

TABLE 3: Averaged Deviations of the Calculated HFPs from the Experimental Ones for Radical R2 According to eqs 9−11[a]

radical	Δa_{iso}^{av}	ΔT_{11}^{av}	ΔT_{22}^{av}	$\lvert\bar{a}_{iso}^{(calc)} - \bar{a}_{iso}^{(exp)}\rvert$
9	8.3	1.0	0.74	0.8
14	8.8	2.3	0.80	7.1
19	19.8	1.2	1.60	4.3

[a] All values are given in MHz.

Let us introduce the following quantities:

$$\bar{a}_{iso} = \frac{1}{3}\sum_{i=1}^{3} a_{iso}(H_N^{(i)}) \quad (9)$$

$$\Delta a_{iso}^{(av)} = \frac{1}{3}\sum_{i=1}^{3} |a_{iso}^{(calc)}(H_N^{(i)}) - a_{iso}^{(exp)}(H_N^{(i)})| \quad (10)$$

$$\Delta T_{kk}^{(av)} = \frac{1}{3}\sum_{i=1}^{3} |T_{kk}^{(calc)}(H_N^{(i)}) - T_{kk}^{(exp)}(H_N^{(i)})|, \quad k = 1, 2 \quad (11)$$

$\bar{a}_{iso}$ is the averaged value of the isotropic HFI constant for three amino protons of radical, and the quantities defined by (10) and (11) are the averaged values of deviations of calculated HFP from the observed ones. According to refs 8 and 9, the parameters $\bar{a}_{iso}$ and $\Delta T_{kk}^{(av)}$ are insensitive to the angle of rotation of the NH_3 group, whereas the value of $\Delta a_{iso}^{(av)}$ is rather sensitive. Table 3 represents these parameters for radicals under consideration. One may see, that radical **9** with the lowest total energy also exhibits a somewhat better agreement of the calculated HFPs with the experiment as compared to the radicals **14** and **19**. It should be noted that HFPs for beta protons of these radicals are rather close to each other and cannot be used for assigning radical R2.

Radicals 10, 15, and 20. These radicals are generated from radicals **3**−**5** by the decarboxylation process. The total energies of these radicals are too high as compared to those of other species. Besides, in contrast to radical **2**, the spin density is fully localized on the CO_2 fragment. Thus, the EPR and ENDOR spectra of such radicals must differ essentially from the ones of the other radicals of the cation branch because of the predicted relatively small HFI with surrounding protons.

From our calculations, it may be deduced that decarboxylation processes in the irradiated alanine crystal are highly improbable. The reasons are (i) the higher total energies of decarboxylation products as compared to the ones of proton-transfer products and (ii) the higher transparency of the potential barrier for proton tunneling.

Thus, radicals **9**, **16**, and **17** are the most probable candidates for those observed by ENDOR radicals R2, R3, and (R3)′.[7] One may notice, however, that our calculations predict the lower total energies for radicals **16** and **17** as compared to that of radical **9**. So, the expected concentration of radicals **16** and **17**, at first glance, must be greater than the concentration of radical **9** in contrast to the experiment.[7] This discrepancy may be caused by two possible reasons. First, the crude model is used for the calculation, leading to invalid relative total energies of the above-mentioned radicals. Second, the potential energy barrier transparency for the proton transfer is larger for radical **9** as compared to that for radicals **16** and **17**, whereas the calculated relative total energies are believed to be correct. The second point of view is supported by the comparison of the distances between H_α and H_o and H_α and H_N in different radicals. Indeed, the calculated distance between H_α in radical **5** and $H_\alpha^{(1)}$ in radical **9** (see Figure 2) is 2.30 Å. At the same, time the calculated distance between H_α in radical **4** and H_o in radical **17** is 4.25 Å. In this case, relative concentrations of the R2 and R3 radicals[7] may depend on the temperature treatment of a crystal during and after irradiation.

It is interesting to consider possible temperature dependence of EPR or ENDOR spectra for radicals of the cation branch. It is well-known that for the anion branch radicals a rather strong temperature dependence of radical structure occurs. At first, the primary anion radical is generated after the trapping of the electron by the neutral alanine molecule and the immediate proton transfer from amino group of the neighbor molecule to the carboxylic group of the radical. It is thought that such a proton transfer is a tunneling process rather than a temperature activated one. This conclusion is based on the experimental fact that the primary anion radical is formed after irradiation at low temperatures. The subsequent significant modification of the anion radical structure at 150° K is caused by a deamination process: the C_α−N bond breaks down and the radical loses the NH_3 group. This phenomenon has distinct features of the temperature activated process.[16] The primary anion radical is long living at low temperatures. At elevated temperatures, the relatively close modifications of the radical structure occur[5] because of some change of dihedral angles.

If we exclude the possibility of the decarboxylation process for the cation branch of the radicals, then one cannot expect a significant temperature dependence of the radical structure. It seems reasonable that radicals **9**, **16**, and **17** will be created immediately even though the crystal is irradiated at low temperature. In this case, intermolecular and intramolecular proton transfer by tunneling may occur simultaneously. It is probable that intermediate species **1**, **3**, **4**, and **5** are short-lived and cannot be observed by means of EPR or ENDOR. However, the existence of the number of various radical conformations with similar structures and almost equal total energies cannot be excluded.

5. Conclusions

The formation of various cation radical structures in the irradiated L-α-alanine crystal is simulated using a 208-atom cluster. The relative total energies and equilibrium geometries of various radical conformations are obtained at the PM3 level. The validity of semiempirical methods for reproducing the hydrogen bond lengths *in the perfect crystal* is tested before such calculations. Different cation radical structures are generated from the primary radical after the amino proton transfer to the neighbor molecules along three distinct hydrogen bonds (deprotonation of the primary radical). This process is accompanied with the intramolecular transfer of an α proton to the amino or carboxylic groups of the radical.

After the deprotonation of the primary radical, the unity positive charge is transferred to the neighbor molecule, and the radical itself becomes neutral. However, in this case, the spin density is completely localized on the corresponding radical. This fact support the final single-point DFT calculation of HFPs for all atoms of the considered radicals. Special attention was paid to the correct simulation of the rotationally averaged HFPs for the protons of the CH_3 group, measured by ENDOR, in the limit of rapid rotation.

Calculations show that radicals with the lowest total energies have the HFPs close to the ones experimentally identified by means of ENDOR radicals R2, R3, and (R3)′.[7]

Moreover, the decarboxylation process for various radical forms is analyzed. Both calculated total energies and HFPs values confirm the point that such a process is highly improbable.

References and Notes

(1) Miyagava, I.; Itoh, K. *J. Chem. Phys.* **1962**, *36*, 2157.
(2) Regulla, D. *Appl. Radiat. Isot.* **2000**, *52*, 1023.
(3) Cassady, C. J.; Carr, S. R.; Zhang, K.; Chung-Phillips, A. *J. Org. Chem.* **1995**, *60*, 1704.
(4) Sinclair, J.; Hanna, M. W. *J. Chem. Phys.* **1969**, *50*, 2125.
(5) Matsuki, K.; Miyagawa, I. *J. Chem. Phys.* **1982**, *76*, 3945.
(6) Kuroda, S.; Miyagawa, I. *J. Chem. Phys.* **1982**, *76*, 3933.
(7) Sagstuen, E.; Hole, E. O.; Haugedal, S. R.; Nelson, W. H. *J. Phys. Chem. A* **1997**, *101*, 9763.
(8) Ban, F.; Wetmore, S. D.; Boyd, R. J. *J. Phys. Chem. A* **1999**, *103*, 4303.
(9) Lahorte, P.; De Proft, F.; Vanhaelewyn, G.; Masschaele, B.; Cauwels, P.; Callens, F.; Geerlings, P.; Mondelaers, W. *J. Phys. Chem. A* **1999**, *103*, 6650.
(10) Friday, E. A.; Miyagava, I. *J. Chem. Phys.* **1971**, *55*, 3589.
(11) Minegishi, A. *J. Phys. Chem.* **1977**, *81*, 1688.
(12) Frisch, M. J.; Trucks, G. W.; Schlegel, H. B.; Gill, P. M. W.; Johnson, B. G.; Robb, M. A.; Cheeseman, J. R.; Keith, T.; Petersson, G. A.; Montgomery, J. A.; Raghavachari, K.; Al-Laham, M. A.; Zakrzewski, V. G.; Ortiz, J. V.; Foresman, J. B.; Cioslowski, J.; Stefanov, B. B.; Nanayakkara, A.; Challacombe, M.; Peng, C. Y.; Ayala, P. Y.; Chen, W.; Wong, M. W.; Andres, J. L.; Replogle, E. S.; Gomperts, R.; Martin, R. L.; Fox, D. J.; Binkley, J. S.; Defrees, D. J.; Baker, J.; Stewart, J. P.; Head-Gordon, M.; Gonzalez, C.; Pople, J. A. *Gaussian 94*, revision E.1; Gaussian, Inc.: Pittsburgh, PA, 1995.
(13) Becke, A. D. *J. Chem. Phys.* **1993**, *98*, 5648.
(14) Lehmann, M. S.; Koetzle, T. F.; Hamilton, W. C. *J. Am. Chem. Soc.* **1972**, *94*, 2657.
(15) Gutowsky, H. S.; McCall, D. W.; Slichter, C. P. *J. Chem. Phys.* **1953**, *21*, 279.
(16) Shields, H.; Hamrick, P. J., Jr.; Smith, C.; Haven, Y. *J. Chem. Phys.* **1973**, *58*, 3420.